Deformation of amorphous silicon nanostructures subjected to monotonic and cyclic loading

C. Gaire, D-X. Ye, T-M. Lu, and G-C. Wang
Department of Physics, Applied Physics and Astronomy, Rensselaer Polytechnic Institute, Troy, New York 12180-3590

R.C. Picu[a)]
Department of Mechanical, Aerospace and Nuclear Engineering, Rensselaer Polytechnic Institute, Troy, New York 12180-3590

(Received 2 March 2007; accepted 29 June 2007)

An atomic force microscope (AFM) was used to characterize the deformation behavior of amorphous Si (a-Si) nanostructures subjected to monotonic and cyclic loading. The sample geometry was specially designed (in the form of elbow) using finite element modeling for the purpose of these tests, and the samples were grown by glancing angle deposition. When deformed monotonically at room temperature, the a-Si specimens exhibited a nonlinear force–displacement response at forces larger than a critical force, a phenomenon not observed in bulk silicon. A fatigue testing methodology based on the use of the AFM was established. The fatigue life of the a-Si specimens was observed to increase by five orders of magnitude with a 50% reduction in the applied force amplitude. It was verified that this delayed failure is caused by progressive damage accumulation during cyclic loading. These results are compared with literature data obtained from micron-size specimens.

I. INTRODUCTION

The increasing use of small micromechanical devices, advanced sensors, biomedical instruments, etc. has not only led to concerns about their long-term reliability issues but has also generated a scientific interest in understanding the deformation mechanisms of these reduced-size structures. The long-term durability is limited by the operation of microscopic mechanisms that allow flaws to develop or existing flaws to grow. Although bulk silicon is not known to exhibit fatigue susceptibility, micron-scale film structures made from silicon are known to degrade during cyclic loading in the ambient.[1] Many studies dedicated to Si are specifically concentrated on evaluating the elastic properties of the crystalline (c-Si) and amorphous (a-Si) material by performing monotonic bending tests of horizontal or slanted nanobeams.[2–5] The elastic properties of these specimens are found to be similar to those of the bulk material. There have been a few but significant studies of the fatigue behavior of microelectromechanical system (MEMS) polysilicon thin-film specimens. These are vibrating structures such as oscillators and comb drives,[6–8] notched cantilever beams,[9] and tensile microspecimens.[10] These studies demonstrated that fatigue behavior of micron-scale specimen is different from that of larger silicon specimens. Two classes of mechanisms have been proposed to explain this observation. The first is based on subcritical cracking in the silicon oxide surface layer (reaction-layer fatigue), while the second is associated with subcritical cracking in the silicon itself. However the issue remains contentious.[11] Nanoindenters and atomic force microscopes (AFM) have enabled the study of mechanical properties of submicron or nanoscale specimens, and there have been a few attempts to evaluate the fatigue properties of c-Si nanowires by the use of AFM based techniques.[3,12] However, such studies are still in their infancy primarily due to the complex instrumentation required.

Monotonic bending and compression tests of metallic micro/nanowires (Ni, Au) have been performed to determine the scaling of the plastic behavior with the specimen size.[13,14] It has been observed that plastic deformation in specimens with at least one dimension smaller than 1 μm is different from that in the macroscopic bulk; specifically, the flow stress is larger and strain hardening is reduced. These changes were attributed to the scarcity of dislocation sources associated with the short travel distance before the defects leave the specimen. This phenomenon was named "dislocation starvation."[15]

[a)]Address all correspondence to this author.
e -mail: picuc@rpi.edu
DOI: 10.1557/JMR.2008.0061

The scaling of the response of brittle amorphous solids with the specimen size was less studied to date. The atomic scale mechanisms of deformation were investigated by computer simulations,[16] and it was shown that stress-mediated interaction of "transformation domains" associated with atomic scale density fluctuations controls localization and potentially, macroscopic failure. Clearly, observing a size effect is expected when the specimen dimensions become comparable to the length scale on which these mechanisms operate.

The purpose of the present study is to investigate the deformation behavior of small volumes of a-Si. The specimens used are grown by oblique angle vapor deposition. They are free-standing nanostructures (in the form of elbows) fixed to the substrate at one end. The load is applied at the free end using an AFM tip. The deformation is also measured using the AFM. We first report the response of the material to monotonic loading, then discuss the development of the AFM-based fatigue test methodology, and lastly consider the fatigue behavior of these structures.

II. EXPERIMENTAL METHODS

A. Sample preparation

The structure used in this study is "elbow" shaped and is shown schematically in Fig. 1(a). The parameters L, b, h, and α denote the average length, width, thickness, and rise angle of the arms (measured from the horizontal). The cross section of the structure is approximately elliptical. The specimens are made from amorphous Si (a-Si) and are fabricated by oblique angle vapor deposition with swing rotation[17] in high vacuum. The setup of the deposition system is described elsewhere.[18,19] The substrate is Si(100) on which tungsten (W) posts of about 450 nm height were deposited by chemical vapor deposition followed by mechanical polishing. The posts are arranged in a square pattern with 1-μm post-to-post distance. The top and bottom diameters of the W posts are about 130 and 360 nm, respectively. The angle, θ, between the vapor direction and the substrate normal was fixed at 85°. The substrate was attached to a stepper motor and was rotated back and forth (swing rotation) at a speed of 1.5×10^{-2} rpm within azimuthal angle $\phi = 90°$ without changing the deposition angle. The pressure during deposition was less than 5×10^{-4} Pa. The deposition rate was determined by a quartz crystal monitor and was 0.50 ± 0.03 nm/s. To grow an elbow structure, a slanted rod (~1 μm in length) was grown to be the first arm. Then, the substrate was rotated by 90° (without changing the angle θ), and another rod of similar dimensions was deposited to make the second arm.

The choice of this sample geometry is due to the observation that in bending tests with slanted nanorods (one arm only),[5] the specimens always failed at the junction between the beam and the substrate. This test would probe the a-Si–W interface and not the a-Si material behavior. These elbow structures were designed to avoid failure at the support and to move the critical region to the turning point of the elbow (point A in Fig. 1). The stress distribution was evaluated by finite element modeling and is discussed further in the Sec. II. B. Hence, the elbow structures are better suited to probe the a-Si response than the simpler, single rodlike geometry.

The grown elbows were imaged by a field emission scanning electron microscopy (FE-SEM-6330F, Jeol Ltd., Tokyo, Japan). Top and side view images were taken and digitized for size analysis. Figures 1(b) and 1(c) show the SEM top and side views of the samples. The average values of α, L, and h were determined from the side view, whereas the average width b was determined from the top view of the images. The dimensions of the elbow structures are: lengths of arms $L_1 = L_2 \approx 1000 \pm 50$ nm, widths of arms $b_1 = b_2 \approx 450 \pm 25$ nm, thicknesses $h_1 = h_2 \approx 250 \pm 25$ nm, and the rise angle from horizontal $\alpha_1 = \alpha_2 \approx 35 \pm 1°$, where the subscripts 1 and 2 denote the first and the second arm, respectively.

B. Mechanical testing

An XE-100 (PSIA Inc., Santa Clara, CA) AFM was used to conduct the monotonic and fatigue tests in air, at room temperature. The force constants of the cantilevers used in the experiments were 35, 37, 38.5, 40.5, and 42.1 N/m (NSC16F series, MikroMasch Ltd., Wilsonville, OR). These were calibrated individually using Sader's method.[20] The Z-piezo detector was calibrated using standard calibration grating. The calibrated force constants and the calibrated Z-detector enable the conversion of the differential photodiode voltage (raw A–B signal) to force. This was done by pushing the tip of the cantilever (cantilever is attached to Z-piezo) a known distance against a sapphire surface while recording the raw A–B signal. To conduct mechanical testing, topographic image of the sample area was taken to locate a particular specimen. The tip was brought in contact with the respective specimen, and the Z displacement of the table was controlled so as to apply a certain force. The force was measured from the cantilever deflection, while the specimen deflection (motion of the point where the force is applied) was calculated by subtracting the cantilever deformation from the Z-motion of the piezo. Hence, the monotonic test is neither force nor displacement controlled. The details of the test procedure are described elsewhere.[5]

Monotonic bending tests were conducted on 34 specimens and the average values for the specimen force constant, k, and the force at failure, F_f, were determined from the force–displacement (F–d) curves. The average force at failure in monotonic tests is also used as a reference for the fatigue tests. The statistics are improved by the fact

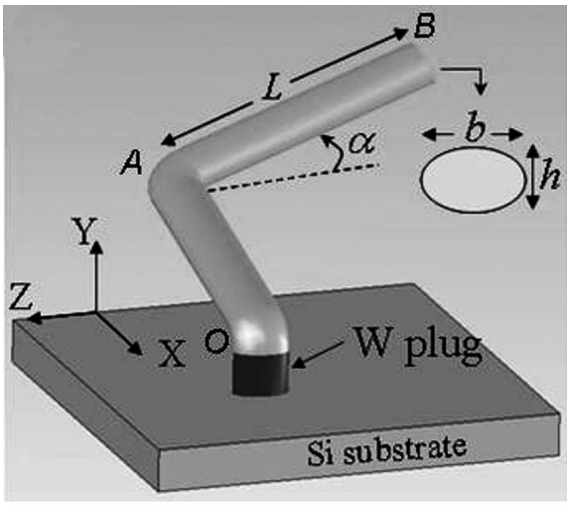

(a)

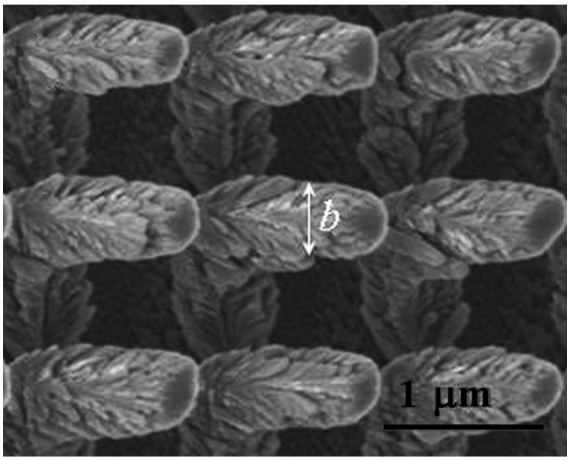

(b)

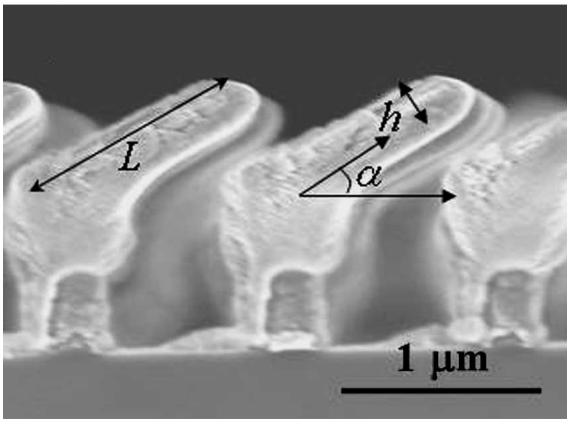

(c)

FIG. 1. (a) Schematic of the test structure (elbow) used in the current experiment. The first arm OA is grown on the W plug and the second arm AB is grown perpendicular to the first arm by rotating the substrate by 90° during deposition. The inset shows the elliptical cross section of the structure with b and h defining the major and minor semiaxes. The dimensions of both arms are similar. (b) The top and (c) the side view SEM images of the a-Si specimens. In (c), the lower arm of the elbow is pointing out of the plane of the image, while the upper arm is in that plane.

that all specimens are quite similar, as all are grown simultaneously.

Fatigue tests were performed by setting the maximum load applied, $F_{max} = 2F_a$. The minimum force of the cycle was 0, and hence the mean load is equal to the cycle amplitude, F_a. The magnitude of the total vertical motion and the loading/unloading speed of the Z-piezo were determined in such a way as to produce the desired frequency of cyclic loading. The cantilever loads the specimen up to $F_{max}\sigma$, which is then held for a short duration of time. The unloading is performed at the same rate as the loading. In all tests reported here, the frequency was 5 Hz. The frequency was kept low to avoid excessive rate effects (if any) in the material response as well as losing the contact between the tip and the specimen. Figure 2 shows the typical time variation of the force applied to the specimen and the Z-piezo displacement. The force curve exhibits the usual snap-in of the cantilever to the specimen, a linear increase of the force, and a plateau corresponding to the Z-piezo hold period, followed by unloading. During the fatigue test, the force and Z-piezo displacement signals were monitored in real time through a LabVIEW (National Instruments Corp., Austin, TX) interface. A large instability in the applied force in a given cycle was interpreted as being caused by specimen failure as discussed in the Results section. A total of 59 specimens were tested in fatigue, and the force versus the number of cycles to failure was plotted. The post-test analysis of the failure surfaces was performed by SEM imaging of the failed specimens.

C. Finite element modeling

Finite element modeling (FEM) of the structure was performed using a commercial software package (ABAQUS; SIMULIA, Providence, RI). The modeling

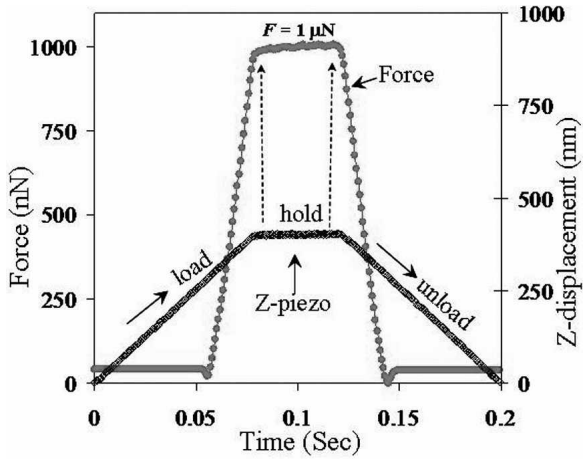

FIG. 2. Time variation of the applied force and the Z-displacement signals from the AFM during a loading–unloading cycle. The force is limited to a specified value (here 1 μN) and is held at the upper limit for a short duration.

was performed to design the specimen geometry for failure to occur at the elbow, as discussed previously. In the model, a distributed force was applied at an angle of 13° (from vertical) at the free end to mimic the finite size and the angle of repose of the AFM tip. The mesh in the vicinity of the turning point of the elbow was refined until the solutions converged. The material was considered elastically isotropic with Young's modulus, $E = 94$ GPa and Poisson's ratio, $\nu = 0.22$.[21] The value of the Young's modulus was measured on the same material (but different specimen geometry) in a separate experiment.[5] It was verified that these values of the elastic constants led to a computed force constant for the structure, k, very close to the measured value.

III. RESULTS AND DISCUSSION

A. Monotonic tests

Figure 3 shows a typical F–d curve obtained in a monotonic test of the elbow structures in Fig. 1. The monotonic F–d curve is linear up to a critical force $F_p \approx 1275 \pm 220$ nN beyond which the linearity breaks down (the uncertainty of the reported figures is associated with tests performed on multiple specimens). The force constant of the specimens, $k = 22 \pm 8$ N/m, was calculated from the linear portion of the F–d curve. The slope of the loading part of the F–d curve decreases beyond the critical force until the force reaches a maximum $F_f \approx 1700 \pm 380$ nN after about 50 nm displacement. Then, the force decreases rapidly, indicating the failure of the specimen. The unloading part of the curve is the cantilever pullout (no response from the specimen) and verifies that the structure failed completely. The complete failure was verified by taking the topographic image of the sample area after each test. The drop of the force beyond the maximum is not abrupt since the piezo continues moving the tip toward the specimen up to point U in Fig. 3, i.e., up to the onset of the retraction period. This feature of the curve occurs because the test is not exactly displacement controlled. Additional information is obtained from the density of data points along the curve. As the points are collected at equal time intervals, the result is that the deformation is stable and performed at constant rate up to the peak of the curve.

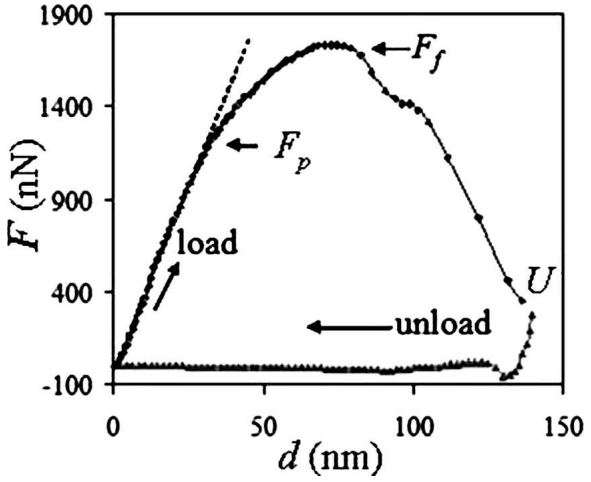

FIG. 3. A typical F-d curve obtained in a monotonic loading test. F_p and F_f indicate the limit of proportionality and the failure force, respectively. Beyond F_f, the specimen fails and the force decreases; however, unloading (retraction of the tip) begins at U.

If the specimens are unloaded before the maximum force F_f is reached, the F–d curve returns to the origin while defining a small hysteresis loop. Reloading takes place on the same path as the initial loading, indicating that no damage accumulated in the specimen. The response to repeated loading–unloading with maximum force within 20% of the failure force F_f has been monitored, and the results are reported in Sec. III. B. 3. As discussed there, the specimen stiffness changes only in the last ~20% of the specimen life. Fully reversible response is measured at all other times.

The maximum measured force F_f corresponds to a maximum principal stress over the entire structure of $\sigma_f = 440 \pm 80$ MPa. The mapping was performed by finite element analysis. This uncertainty in the stress amplitude is associated with the scatter in the value of F_f and with the uncertainty in the dimensions of the specimens (determined from SEM images). For polycrystalline silicon the measured fracture stress varies with processing conditions and grain size and was reported to be between 1 and 4 GPa.[22–24] Thus, it can be observed that the monotonic fracture stress for these a-Si specimens is approximately an order of magnitude smaller, compared with the polysilicon specimens.

B. Fatigue tests

1. Fatigue failure identification

Figures 4(a) and 4(b) show typical force and Z-motion waveforms, respectively, obtained from the nanoscale fatigue tests on the a-Si elbow structure. The force waveform is approximately constant over the entire test duration except in the final cycle when the specimen fails. When the specimen fails completely, the force drops toward 0, but because of the large value of the Z-displacement, the AFM cantilever hits and loads the substrate. This results in two clear peaks in the force waveform; the first is the specimen response, and the second is the substrate response. In Fig. 4, the failure occurs in 4620th cycle as indicated by the two peaks in the force waveform. This method of monitoring the failure of the specimen in real time is novel. To ensure that the double-peak phenomenon described previously is not an artifact, AFM topographic images of the sample area before and after the tests were taken. Figure 5(a) shows the AFM image of the sample area before the fatigue test. The

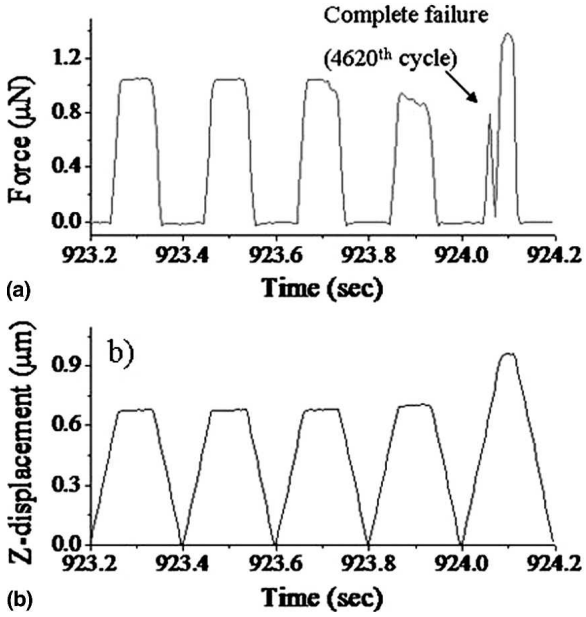

FIG. 4. (a) Force waveform and (b) the accompanying Z-displacement plotted against time showing the failure of the specimen. In this particular test, a peak force of 1050 nN was used and the failure resulted in the 4620th cycle as indicated by the instability in force as well as Z-displacement waveforms. The first of the two peaks in the last cycle corresponds to the response from the specimen, the dip corresponds to failure, while the second peak is due to the cantilever loading the substrate.

specimen marked with "X" was loaded cyclically. Once the fluctuation in the force level described here was noted, the loading was stopped and a topographic image was taken [Fig. 5(b)]. The specimen marked by "X" in Fig. 5(a) is missing in Fig. 5(b), indicating its complete failure. The procedure was repeated for all specimens tested. It was also verified that if the test is stopped before the double peak in the force waveform is observed; all specimens appear intact upon topographic imaging.

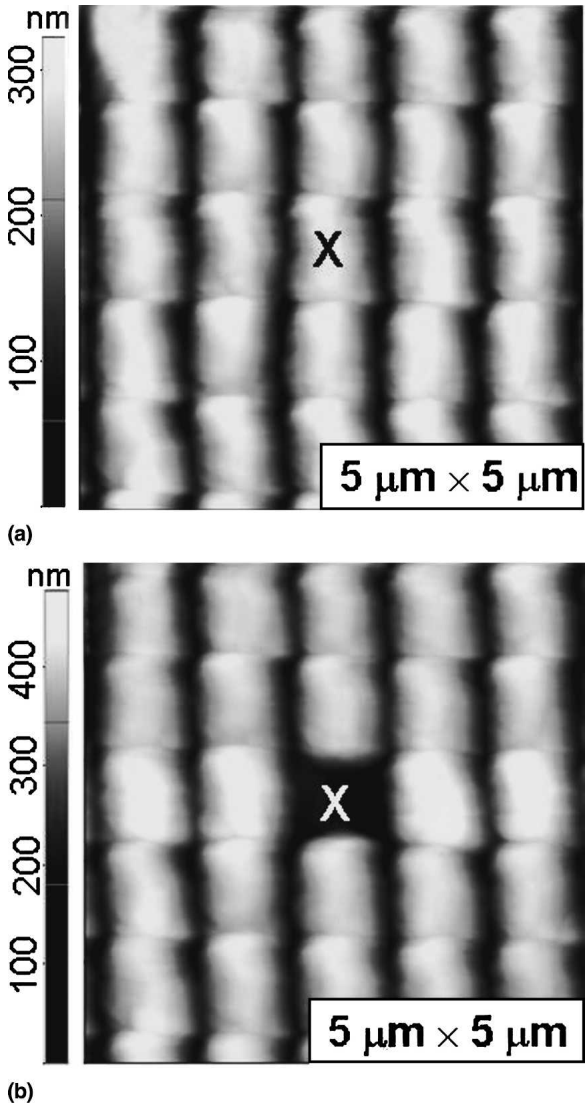

FIG. 5. Topographic AFM images of the sample area (a) before and (b) after the cyclic test. The specimen marked by "X" in (a) is loaded and fails, so is not present in (b).

2. Fatigue life curve

Figure 6 depicts the ratio of the peak applied force to the monotonic failure force (F/F_f) versus the number of cycles to failure. The number of cycles to failure (N_f) data were collected with force amplitudes ranging from ~40% to 100% of F_f. The number of cycles to failure values range from $N_f = 1$ to 2.7×10^5 cycles at $F/F_f \approx 1$ to 0.44, respectively. The fatigue lifetime of the a-Si structures is observed to increase monotonically with decreasing force. With a 50% reduction in applied peak force (to ~800 nN), the lifetime increases by approximately 5 orders of magnitude. Through FEM, this force translates into a maximum principal stress value of ~210 MPa at the turning point of the elbow.

The bulk silicon is inherently brittle at room temperature and is not susceptible to fatigue due to extremely low dislocation activity at low homologous temperature,[25] little or no extrinsic toughening mechanism,[26] and susceptibility to environmentally assisted cracking.[27] However, micron-scale polycrystalline silicon was observed to show some delayed failure during cyclic loading.[9] For example, in Ref. 9 it is reported that for a polysilicon specimen (~2 μm thick with grain size ~200 nm), a 50% reduction in stress amplitude (to ~2 GPa) resulted in an increase in life of approximately five orders of magnitude. The fatigue process was attributed to the environmentally assisted cracking of the surface oxide layer (reaction-layer fatigue). Note that the nanoscale a-Si specimens used in our experiments show a similar extension of the fatigue life; however, they fail in cyclic loading at an order of magnitude lower stress (~200 MPa) compared with the polysilicon specimens. A systematic investigation of the grain size dependence of

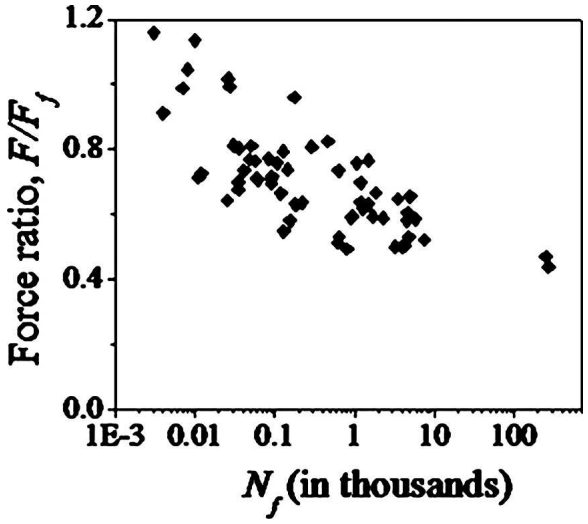

FIG. 6. The variation of fatigue life (number of cycles to failure) with the applied maximum force, F. The amplitude and the mean of the cycle are both equal to $F/2$. The vertical axis is normalized by the monotonic failure force, F_f (Fig. 3).

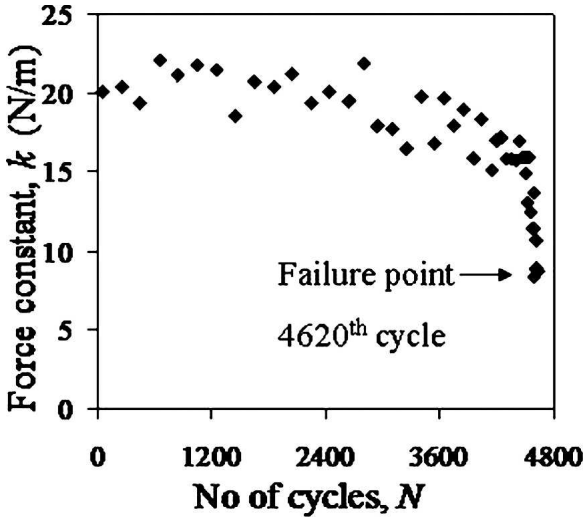

FIG. 7. The variation of the measured specimen stiffness, k, during cyclic loading. Initially the stiffness was evaluated every 200th cycle, after ~$0.7N_f$ every 50th cycle, and after ~$0.9N_f$ every 10th cycle. The stiffness is approximately constant up to ~$0.8N_f$, while in the final ~$0.2N_f$ cycles it decreases abruptly.

the fatigue crack growth rate[28] in alumina with the grain size varying from 1 to 30 μm suggests that even though the crack growth rate is insensitive to the grain size, the stress intensity threshold at which cracks start to propagate, K_{th}, is lower in the small grained material. This trend is in agreement with the result presented here.

The presence of native oxide layer on the silicon surface is inevitable since the experiments were carried out in the ambient environment. For single-crystal silicon, the oxide layer thickness is on the order of 1 nm. For amorphous Si nanostructures, we also expect the existence of an oxide layer on the surface, but its thickness was not measured.

3. Damage evaluation

Fatigue experiments have established that changes in resonant frequency of the structure (in tests performed at resonance, with MEMS) are a result of progressive damage accumulation during cyclic loading.[29] The force constant of our specimens was evaluated from the measured F–d data every few cycles to monitor damage accumulation during the tests. Figure 7 shows a typical variation of the measured force constant with the number of cycles. As usually observed in fatigue at the macroscopic scale, damage seems to accumulate slowly (the variation of the force constant is comparable with the scatter in the data) up to ~80% of the number of cycles to failure. Damage accumulates at a much faster rate in the last 20% of the specimen life. This is an interesting observation in a nanoscale specimen as in large-scale samples the long incubation period is associated with the nucleation of nano/microscale cracks.

4. Failure analysis

Figures 8(a) and 8(b) show SEM images of the failed samples that have been subjected to cyclic loading. In most cases, the sample failed from the turning point of

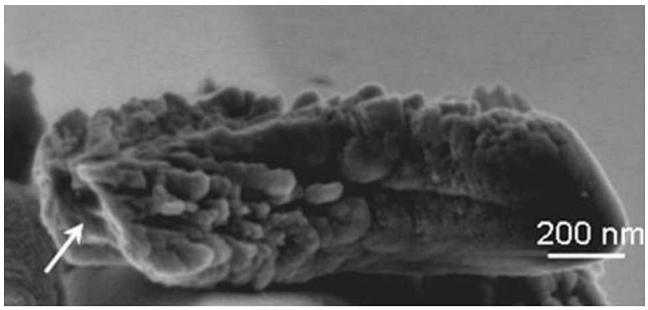

(a)

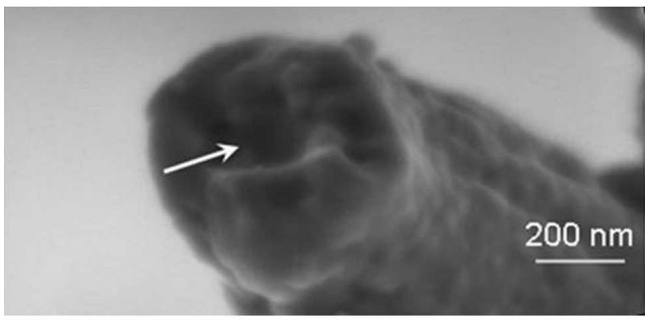

(b)

FIG. 8. Failure surfaces (indicated by white arrows) of the elbow structure subjected to fatigue loading. (a) The failure surface on the upper arm of the elbow structure. (b) The failure surfaces on the lower arm of the structure (different specimens). Note that the failure surfaces are rough and there are no signs of ductility.

the elbow (point A in Fig. 1). The arrows show the fracture surfaces in the upper and lower arms, respectively (of different specimens). The failure surfaces run at an angle of approximately 45° with respect to the rod axis. There is no obvious sign of ductile fracture.

Figures 9(a) and 9(b) show the maximum principal and maximum shear stress distribution evaluated using FEM and corresponding to an applied peak force of 1000 nN. As discussed before, both stresses are highest at the turning point of the elbow. However, the maximum principal stress (tensile) is approximately 1.5 times higher than the shear stress. Also, the normal stress acts approximately perpendicular to the direction shown by the dotted line *FF′*, which is also the plane of failure observed fractographically. The maximum shear stress results at a location close to that of the maximum normal stress [Fig. 9(b)]. The stress distribution exhibits very large gradients in all directions, including in the across-thickness direction of the failure plane, due to the small dimensions of these samples. Hence, a definite conclusion on the failure mechanism and the stress component that controls it is premature. It can also be observed that the specimen surface is rather rough [Fig. 8(a)], and these asperities, although very small, may lead to stress concentration. These aspects are currently considered by means of modeling. In particular, we are interested in determining how these large stress gradients interact with the atomic scale structural variability of the amorphous material (spatial density fluctuations). This discussion is deferred to a separate publication.

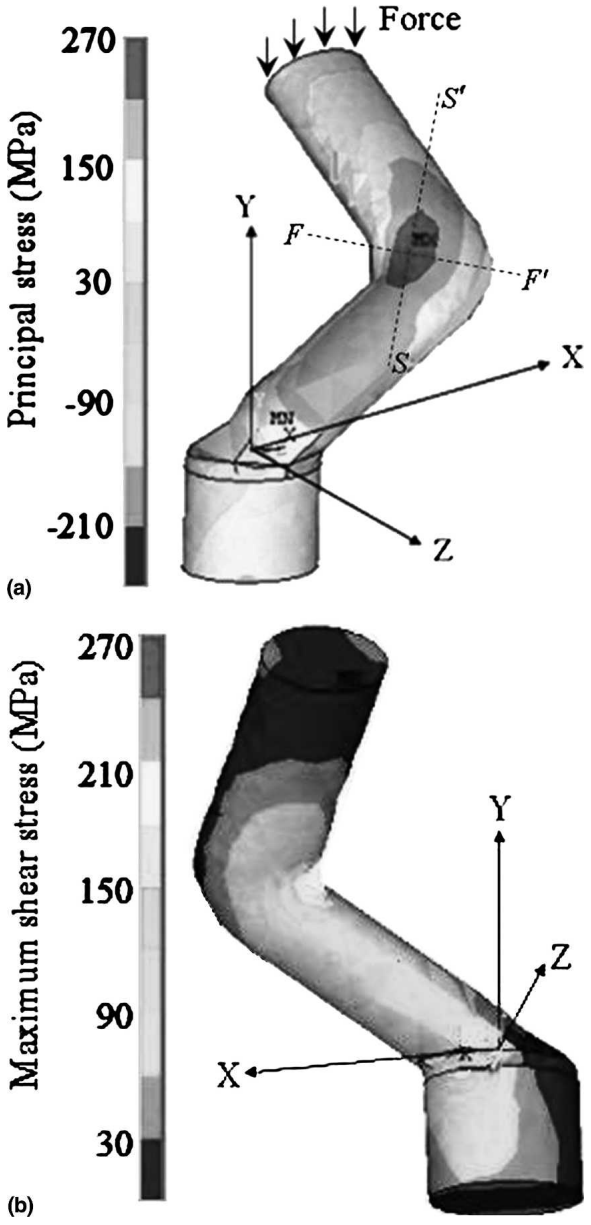

FIG. 9. (a) Maximum principal and (b) maximum shear stress distributions obtained by finite element modeling and corresponding to an applied force of 1000 nN. The dotted line *SS′* represents the direction in which the maximum tensile principal stress acts, while the dotted line *FF′* shows the approximate failure plane observed in experiments. Note that both stresses are highest at the turning point of the elbow [A in Fig. 1(a)].

It has been shown that the sample preparation method has a large effect on the density of the a-Si films.[30] The mechanical properties of the a-Si nanostructures are also expected to be somewhat sensitive to the sample preparation method. Nevertheless, the fundamental deformation mechanisms are expected to be insensitive to these parameters. Hence, results obtained with specimens grown under different conditions are expected to exhibit trends similar to those discussed here, though some quantitative variations are possible.

IV. CONCLUSIONS

The deformation behavior of a-Si nanostructures grown by oblique angle physical vapor deposition was characterized with the use of AFM. In the monotonic tests, the specimens were observed to exhibit nonlinear deformation before failure. A fatigue test methodology based on the use of the AFM was established, and a novel method for determining the occurrence of complete failure was used. The fatigue life of the a-Si specimens was observed to increase by 5 orders of magnitude with a 50% reduction in the applied force amplitude. The comparison with published data obtained with larger specimens suggests that fatigue susceptibility increases with decreasing sample size. It was verified that this delayed failure is caused by progressive "damage" accumulation during cyclic loading, a surprising conclusion for a nanoscale specimen. Despite the expectations based on the observation of nonlinear deformation under monotonic loading and of progressive damage accumulation during cyclic loading, signs of ductile failure could not be evidenced on the fracture surfaces.

ACKNOWLEDGMENTS

This material is based on work supported by the National Science Foundation under Grant No. 0324492. Any opinions, findings, and conclusions or recommendations expressed in this material are those of the authors and do not necessarily reflect the views of the NSF. We thank F. Tang, T. Parker, M.A. Soare, and P. Morrow for various help during the experiment.

REFERENCES

1. C.L. Muhlstein, R.T. Howe, and R.O. Howe: Fatigue of polycrystalline silicon for microelectromechanical systems applications: Crack growth and stability under resonant loading conditions. *Mech. Mater.* **36,** 13 (2004).
2. T. Namazu, Y. Isono, and T. Tanaka: Evaluation of size effect on mechanical properties of single-crystal silicon by nanoscale bending test using AFM. *J. Microelectromech. Sys.* **9,** 450 (2000).
3. S. Sundararajan and B. Bhushan: Development of AFM-based techniques to measure mechanical properties of nanoscale structures. *Sens. Actuators, A* **101,** 338 (2002).
4. K.R. Virwani, A.P. Malshe, W.F. Schmidt, and D.K. Sood: Young's modulus measurements of silicon nanostructures using a scanning probe system: A nondestructive evaluation approach. *Smart Mater. Struct.* **12,** 1028 (2003).
5. C. Gaire, D-X. Ye, F. Tang, R.C. Picu, G-C. Wang, and T-M. Lu: Mechanical testing of isolated amorphous silicon slanted nanorods. *J. Nanosci. Nanotechnol.* **5,** 1893 (2005).
6. H. Kahn, R. Ballarini, R.L. Mullen, and A.H. Heuer: Electrostatically actuated failure of microfabricated polysilicon fracture mechanics specimens. *Proc. R. Soc. (London)* **455,** 3807 (1999).
7. J.A. Connally and S.B. Brown: Micromechanical fatigue testing. *Exp. Mech.* **33,** 81 (1993).
8. K. Komai, K. Minoshima, and S. Inoue: Fracture fatigue behavior of single crystal silicon microelements and nanoscopic AFM damage evaluation. *Microsyst. Technol.* **5,** 30 (1998).
9. C.L. Muhlstein, S.B. Brown, and R.O. Ritchie: High-cycle fatigue and durability of polycrystalline silicon thin films in ambient air. *Sens. Actuators, A* **94,** 177 (2001).
10. T. Ando, M. Shikida, and K. Sato: Tensile-mode fatigue testing of silicon films as structural materials for MEMS. *Sens. Actuators, A* **93,** 70 (2001).
11. D.H. Alsem, O.N. Pierron, E.A. Stach, C.L. Muhlstein, and R.O. Ritchie: Mechanisms for fatigue of micron-scale silicon structural films. *Adv. Eng. Mater.* **9,** 15 (2007).
12. T. Namazu and Y. Isono: High cycle fatigue damage evaluation for micro-nanoscale single crystal silicon under bending and tensile stressing, in *Micro-Electro-Mechanical Systems* (17th IEEE Int. Conf. Proc., New York, 2004), p. 149.
13. M.D. Uchic, D.M. Dimiduk, J.N. Florando, and W.D. Nix: Sample dimensions influence strength and crystal plasticity. *Science* **305,** 986 (2004).
14. B. Wu, A. Heidelberg, and J.J. Boland: Mechanical properties of ultrahigh strength gold nanowires. *Nat. Mater.* **4,** 525 (2005).
15. J.R. Greer, W.C. Oliver, and W.D. Nix: Size dependence of mechanical properties of gold at the micron scale in the absence of strain gradients. *Acta Mater.* **53,** 1821 (2005).
16. M.J. Demkowicz and A.S. Argon: High-density liquidlike component facilitates plastic flow in a model amorphous silicon system. *Phys. Rev. Lett.* **93,** 025505 (2004).
17. D-X. Ye, Y-P. Zhao, G-R. Yang, Y-G. Zhao, G-C. Wang, and T-M. Lu: Manipulating the column tilt angles of nanocolumnar films by glancing angle deposition. *Nanotechnology* **13,** 615 (2002).
18. Y-P. Zhao, D-X. Ye, G-C. Wang, and T-M. Lu: Novel nanocolumn and nano-flower arrays by glancing angle deposition. *Nano Lett.* **2,** 351 (2002).
19. D-X. Ye, T. Karabacak, R.C. Picu, G-C. Wang, and T-M. Lu: Uniform Si nanostructures grown by oblique angle deposition with substrate swing rotation. *Nanotechnology* **16,** 1717 (2005).
20. J.E. Sader, J.W.M. Chon, and P. Mulvanev: Calibration of rectangular atomic force microscope cantilevers. *Rev. Sci. Instrum.* **70,** 3967 (1999).
21. L.B. Freund and S. Suresh: *Thin Film Materials,* 1st ed. (Cambridge University Press, Cambridge, UK, 2003), p. 96.
22. W.N. Sharpe, Jr. and J. Bagdahn: Fatigue testing of polysilicon—A review. *Mech. Mater.* **36,** 3 (2004).
23. W.N. Sharpe, Jr., K. Jackson, G. Coles, and D.A. LaVan: Mechanical properties of different polysilicons, in *Micro-Electro-Mechanical Systems* (ASME Int. Mechanical Engineering Congress Expo. 5–10, Orlando, FL, 2000), p. 255.
24. O.N. Pierron, C.C. Abnet, and C.L. Muhlstein: Methodology for low-and high-cycle fatigue characterization with kHz-frequency resonators. *Sens. Actuators, A* **128,** 140 (2006).
25. K. Sumino: Deformation behavior of silicon. *Metall. Mater. Trans. A* **30,** 1465 (1999).
26. H. Kahn, N. Tayebi, R. Ballarini, R.L. Mullen, and A.H. Heuer: Fracture toughness of polysilicon MEMS devices. *Sens. Actuators, A* **82,** 274 (2000).
27. T.J. Chen and W.J. Knapp: The fracture of single crystal silicon under several liquid environments. *J. Am. Ceram. Soc.* **63,** 225 (1980).
28. C.J. Gilbert and R.O. Ritchie: Mechanisms of cyclic fatigue-crack propagation in a fine-grained alumina ceramic: Role of crack closure. *Fatigue Fract. Eng. Mater. Struct.* **20,** 1453 (1997).
29. W.W. van Arsdell and S.B. Brown: Subcritical crack growth in silicon MEMS. *J. Microelectromech. Sys.* **8,** 319 (1999).
30. T.A. Hayes and M.E. Kassner: Elastic constants of a-Si and a-Si:H, in *Properties of Amorphous Si and Its Alloys,* edited by Tim Searle (INSPEC Publication, The Inst. Electrical Engineers, London, UK, 1998), p. 359.